

Article

# Reduction of Defects in AlGa<sub>N</sub> Grown on Nanoscale-Patterned Sapphire Substrates by Hydride Vapor Phase Epitaxy

Chi-Tsung Tasi <sup>1</sup>, Wei-Kai Wang <sup>2</sup>, Tsung-Yen Tsai <sup>1</sup>, Shih-Yung Huang <sup>3</sup>, Ray-Hua Horng <sup>4</sup> and Dong-Sing Wu <sup>1,\*</sup>

<sup>1</sup> Department of Materials Science and Engineering, National Chung Hsing University, Taichung 40227, Taiwan; d100066018@mail.nchu.edu.tw (C.-T.T.); d9566208@alumni.nchu.edu.tw (T.-Y.T.)

<sup>2</sup> Department of Materials Science and Engineering, Da-Yeh University, Changhua 51591, Taiwan; wk@mail.dyu.edu.tw

<sup>3</sup> Department of Industrial Engineering and Management, Da-Yeh University, Changhua 51591, Taiwan; syh@mail.dyu.edu.tw

<sup>4</sup> Department of Electronics Engineering, National Chiao Tung University, Hsinchu 300, Taiwan; rhh@nctu.edu.tw

\* Correspondence: dsw@nchu.edu.tw; Tel.: +886-4-2284-0500 (ext. 714); Fax: +886-4-2285-5046

Academic Editor: Lioz Etgar

Received: 10 April 2017; Accepted: 29 May 2017; Published: 31 May 2017

**Abstract:** In this study, a 3- $\mu\text{m}$ -thick AlGa<sub>N</sub> film with an Al mole fraction of 10% was grown on a nanoscale-patterned sapphire substrate (NPSS) using hydride vapor phase epitaxy (HVPE). The growth mechanism, crystallization, and surface morphology of the epilayers were examined using X-ray diffraction, transmission electron microscopy (TEM), and scanning electron microscopy at various times in the growth process. The screw threading dislocation (TD) density of AlGa<sub>N</sub>-on-NPSS can improve to  $1\text{--}2 \times 10^9 \text{ cm}^{-2}$ , which is significantly lower than that of the sample grown on a conventional planar sapphire substrate ( $7 \times 10^9 \text{ cm}^{-2}$ ). TEM analysis indicated that these TDs do not subsequently propagate to the surface of the overgrown AlGa<sub>N</sub> layer, but bend or change directions in the region above the voids within the side faces of the patterned substrates, possibly because of the internal stress-relaxed morphologies of the AlGa<sub>N</sub> film. Hence, the laterally overgrown AlGa<sub>N</sub> films were obtained by HVPE, which can serve as a template for the growth of ultraviolet III-nitride optoelectronic devices.

**Keywords:** AlGa<sub>N</sub>; hydride vapor phase epitaxy (HVPE); nanoscale-patterned sapphire substrate (NPSS); dislocation density (TD)

## 1. Introduction

Recently, the use of epitaxial Al<sub>x</sub>Ga<sub>1-x</sub>N alloys wide-band gap semiconductors have drawn increasing attention because of their potential expanding applications for ultraviolet (UV) optoelectronic devices and high-power, high-frequency electronic devices [1–3]. However, the dislocation density within UV optoelectronic devices significantly affects their internal quantum efficiency and operational lifetime due to the presence of heteroepitaxial-growth-induced defects (e.g., threading dislocations (TDs), stacking faults, voids, and point defects) [4,5]. Hence, the epitaxial growth of high quality AlGa<sub>N</sub> materials plays an important role in determining the performance of AlGa<sub>N</sub>-based devices.

Hydride vapor phase epitaxy (HVPE) has been shown to achieve rapid growth rates of several hundred micrometers per hour. Growth rates of approximately 30–50  $\mu\text{m}/\text{h}$  have been reported for the growth of freestanding GaN substrates and AlN [6,7]. Therefore, HVPE is expected to permit the growth of thick AlGa<sub>N</sub>, which can possibly serve as pseudosubstrates to mitigate the lack of

suitable substrates for the growth of low-defect AlGa<sub>x</sub>N wafer. However, AlGa<sub>x</sub>N pseudosubstrates are not currently available because of practical fabrication challenges, including crack formation within the Al<sub>x</sub>Ga<sub>1-x</sub>N layer grown on foreign substrates, inhomogeneous Al incorporation at different facets, and parasitic reactions [8]. Al-containing material tends to react violently with SiO<sub>2</sub> during growth, and thus a SiO<sub>2</sub> mask is forbidden to use for AlGa<sub>x</sub>N epitaxial lateral overgrowth (ELOG). To address these issues, patterned sapphire substrates (PSSs) are promising substrate materials for the direct lateral epitaxial growth of AlGa<sub>x</sub>N using HVPE [9,10]. Hedagorn et al. reported the successful growth of a smooth 40- $\mu$ m-thick Al<sub>0.45</sub>Ga<sub>0.55</sub>N layer on a trench-shaped PSS. They also investigated the effect of the total pressure, V/III ratio, and substrate miscut direction on the growth of AlGa<sub>x</sub>N on a trench-shaped PSS [11,12]. Kuwano et al. showed that the main problem in ELOG is predominantly caused by the grain growth along different orientations on the sidewalls of the patterned substrates [13]. Richter et al. discussed the growth behavior of an Al<sub>0.3</sub>Ga<sub>0.7</sub>N layer grown on a honeycomb-shaped PSS [14]. They observed that nanometer-scaled patterns rather than micrometer-scale stripe patterns are more suitable for the extraction of UV emitter light through the substrate. Furthermore, patterned structures extending to the nanoscale (submicron) are more effective in reducing the number of TDs by bending the dislocation direction to the sidewalls of the patterned template [15]. In this study, an overgrown high-quality AlGa<sub>x</sub>N layer was directly grown on nanoscale-PSSs (NPSSs) using HVPE without the use of complex processes. In addition, the growth mechanism and material properties of the AlGa<sub>x</sub>N were investigated as a function of growth time.

## 2. Materials and Methods

Two-inch c-plane sapphire substrates were used as the starting materials for the NPSSs. A low-pressure chemical vapor-deposited SiO<sub>2</sub> film on sapphire served as the mask layer, which the nano-imprint resist was spin-coated on. The hexagonal hole array was transferred to the resist by nano-imprint lithography, followed by oxygen plasma descum to removing any residual resist at the bottom of the holes. The SiO<sub>2</sub> film was then etched by a fluorine plasma. Finally, a BCl<sub>3</sub>/Cl<sub>2</sub> high-density-plasma etching process was employed to etch the sapphire substrate, and the mask was removed by a dilute HF solution. Although a variety of hole dimensions for nano-imprinting were attempted, the optimum NPSSs used in this study were with 500-nm-diameter hole array, spaced 950 nm apart, and etched to a depth of 400 nm.

The growth of the AlGa<sub>x</sub>N epilayer on NPSS or conventional sapphire substrate (CSS) was performed using a HVPE horizontal reactor as shown schematically in Figure 1. The quartz glass reactor was covered with a furnace containing five heating zones maintained at different temperatures. Ga and Al metal chlorides serving as the group III Ga and Al precursor sources, respectively, were separately placed in the upstream region of the quartz reactor. The AlCl<sub>3</sub> and GaCl vapors were generated in the reactor by flowing HCl over the Al (10 sccm) and Ga precursor (10 sccm) sources, respectively. To avoid the formation of AlCl vapor by a reaction between the Al metals and HCl at high temperature (which would damage the quartz reactor), the Al metal source was maintained at 500 °C to ensure the sole formation of AlCl<sub>3</sub> vapor. The temperature of the GaCl source was maintained between 800 °C and 900 °C. Pure N<sub>2</sub> gas (400 sccm) served as the carrier gas to propel the AlCl<sub>3</sub> and GaCl vapors through two quartz tubes to the growth zone. The ammonia line consists of the NH<sub>3</sub> flow (2 L/min) and N<sub>2</sub> flow (300 sccm). During the HVPE process, the H<sub>2</sub> flow was kept at 2.45 L/min, N<sub>2</sub> flow at 200 sccm, growth pressure at 200 mbar, and growth temperature at 1080 °C. Transmission electron microscopy (TEM, JEM-2010, JEOL, Tokyo, Japan), scanning electron microscopy (SEM, S-3000H, Hitachi, Tokyo, Japan), atomic force microscopy (AFM, 5400, Agilent, Santa Clara, CA, USA), double-crystal x-ray diffraction (DCXRD, X'Pert PRO MRD, PANalytical, Almelo, The Netherlands), and photoluminescence (PL, Fluoromax-3, Horiba, Tokyo, Japan) measurements were conducted to examine the microstructure and optical properties of the AlGa<sub>x</sub>N epilayers grown on the NPSSs.

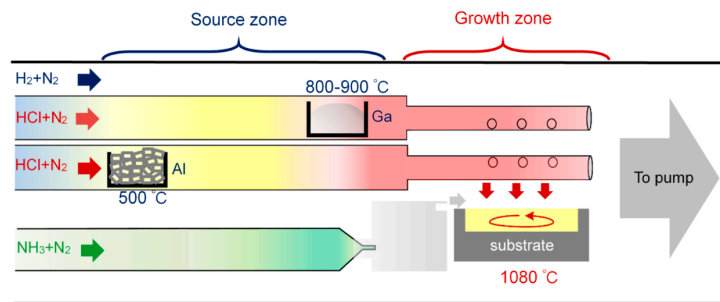


**Figure 1.** Schematic diagram of the hydride vapor phase epitaxy (HVPE) reactor used for the AlGa<sub>N</sub> growth.

### 3. Results and Discussion

Schematic illustrations of the top- and side-view dimensions of the NPSS design are shown in Figure 2a,b, respectively. A typical surface morphology of the as-etched NPSS examined by scanning electron microscopy (SEM) is shown in Figure 2c. To study the patterned substrate effect, the HVPE growth of the Al<sub>x</sub>Ga<sub>1-x</sub>N with an Al mole fraction of  $x = 0.1$  (“AlGa<sub>N</sub>” hereafter) on NPSS was proceeded. A CSS was also used in these experiments.

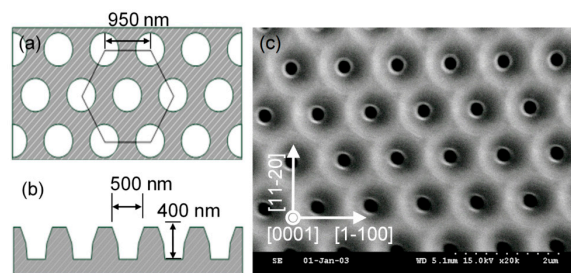


**Figure 2.** Schematic illustrations of the (a) top- and (b) side-view dimensions of the nanoscale- patterned sapphire substrate (NPSS) design used in this study. (c) SEM surface morphology of the as-etched NPSS.

The SEM surface morphologies of the AlGa<sub>N</sub> films grown on both the CSS and NPSS are shown in Figure 3a,b, respectively. The AlGa<sub>N</sub> on CSS exhibited a hexagonal-shape faceting structure, resulting in a rough surface. In contrast, the AlGa<sub>N</sub> film grown on an NPSS shows a relatively smooth and uniform surface. A comparison of the transmittance spectra of AlGa<sub>N</sub> grown on both the CSS and NPSS is shown in Figure 3c. The optical absorption edge at  $360 \pm 5$  nm corresponds to an Al mole fraction of 10 at %, which is consistent with our double-crystal X-ray diffraction (DCXRD) measurements. In general, the AlGa<sub>N</sub> layer on the NPSS exhibited reduced transmissivity, which is thought to be caused by light scattering via the NPSS and reflections caused by air voids embedded at the interface between the AlGa<sub>N</sub> and sapphire interface [10].

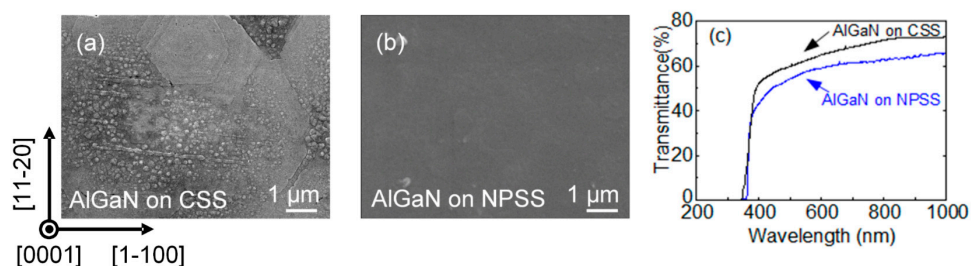


**Figure 3.** SEM surface morphologies of the AlGa<sub>N</sub> epilayers grown on the (a) conventional sapphire substrate (CSS) and (b) NPSS. The corresponding transmittance spectra are shown in (c).

To study the nanoheteroepitaxial growth of AlGa<sub>N</sub>-on-NPSS, the growth evolution with various growth periods were identified by cross-sectional SEM images. Figure 4a–d show the AlGa<sub>N</sub> films grown on NPSSs at growth times of 5, 10, 20, and 30 min. For the initial growth times of 5 and 10 min, the AlGa<sub>N</sub> films began to grow from the NPSS sidewall of m-plane facets (Figure 4a–b). The selective growth of the AlGa<sub>N</sub> layer is possibly related to the different migration rates of Ga atoms on the (0001) and {11–2k} facets during the HVPE growth process. With time, the AlGa<sub>N</sub> coalesced, resulting in the formation of an epitaxial lateral overgrowth (Figure 4c). Finally, after 30 min, a flat 3-μm-thick AlGa<sub>N</sub> epilayer on a NPSS with small voids at the interface is shown in Figure 4d–e with different magnifications.

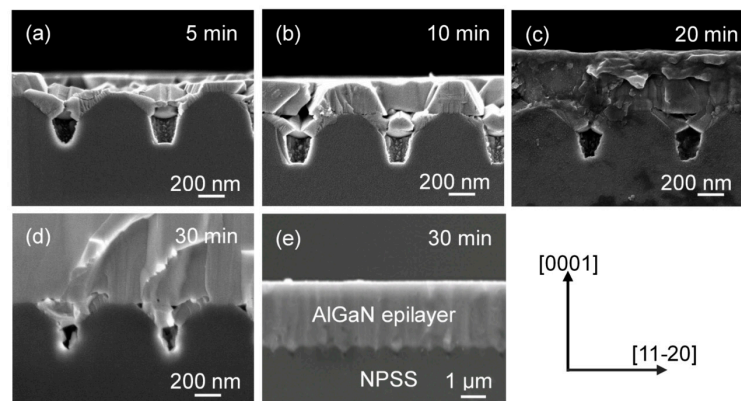


**Figure 4.** Cross-sectional SEM images of the AlGa<sub>N</sub> epilayers on NPSSs for various growth times ((a–d) 5, 10, 20, and 30 min); (e) are micrographs of the same 3-μm-thick cross-sectional AlGa<sub>N</sub>-on-NPSS sample (30 min) with different magnifications.

The corresponding surface roughnesses of these samples were examined by atomic force microscopy using a scan area of 100 μm<sup>2</sup>. As shown in Figure 5, the surface root-mean-square (RMS) roughness values of these samples were measured to be 44.5, 26.5, 11.6, and 7.52 nm for growth times of 5, 10, 20, and 30 min, respectively. The AFM results indicate that the surface of the AlGa<sub>N</sub> film on the NPSS was relatively smooth and did not contain surface pits at a growth time of 30 min.

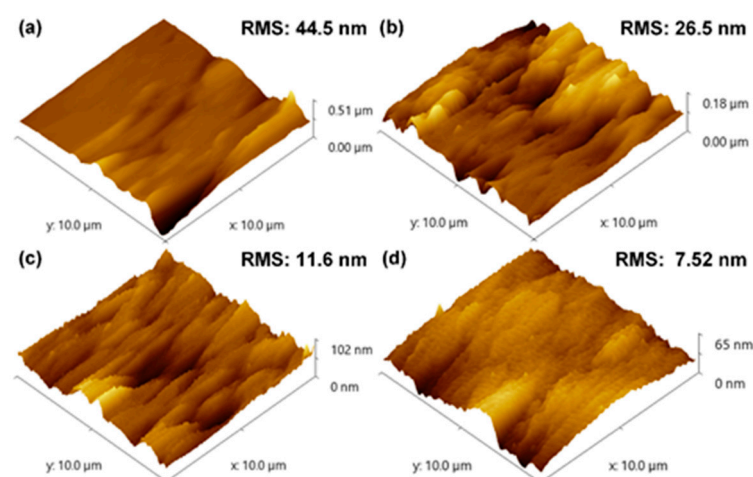


**Figure 5.** Atomic force microscopy (AFM) measurement of AlGa<sub>N</sub> grown on an NPSS at growth times of (a) 5; (b) 10; (c) 20 and (d) 30 min. RMS: root-mean-square.

Based on these observations, a schematic growth evolution mechanism of the AlGa<sub>N</sub> ELOG structure on the NPSS is proposed and shown in Figure 6. The large overgrowth formation would lead

to a reduction in the TD density in the overlayer region. However, the AlGa<sub>N</sub> film formed at an initial growth time of 5 min exhibited a very rough surface, indicating an incomplete 3D-island-coalescence growth process. This result is consistent with the SEM results presented in Figure 4a.

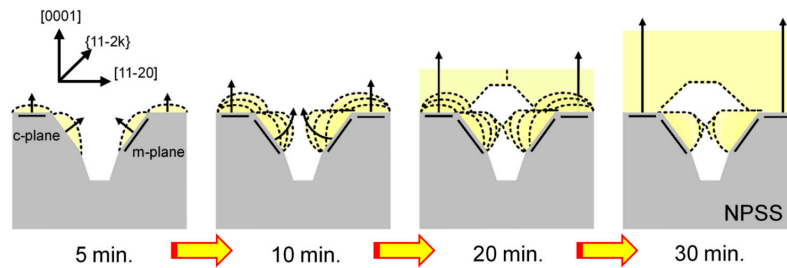


**Figure 6.** AFM measurement of AlGa<sub>N</sub> grown on a NPSS at growth times of 5, 10, 20, and 30 min.

Figure 7a shows the DCXRD full-width half-maximum (FWHM) results with the symmetric (002) and asymmetric (102) planes for the AlGa<sub>N</sub> samples as demonstrated in Figure 4. The FWHM values of the (002) and (102) reflections decreased with increasing growth time from 5 to 30 min. At a growth time of 30 min, narrower FWHM values of 1000 and 2500 arcsec were obtained for the (002) and (102) reflections, respectively, indicating that the quality of the AlGa<sub>N</sub> epilayer improved for a lower TD density. Furthermore, the symmetric (002) and (102) reflections can provide information on the density of pure screw and pure edge TDs, respectively. The reflection was brought into the diffraction condition by rotating the crystal's surface normal out the diffraction plane by an angle  $\chi$ . Here the angle  $\chi$  was measured at 48.08 between the reciprocal lattice vector ( $K_{hkl}$ ,  $hkl = 102$ ) and (001) surface normal. Specifically, the density of screw dislocations  $\rho_s$  could be calculated using the following equation:

$$\rho_s = \frac{\beta_{\text{tilt}}^2}{4.35b_c^2} \quad (1)$$

where  $b_c$  is the Burgers vector of c-type TDs ( $b_c = 0.5185$  nm) and the FWHM values of (002) reflection were used to evaluate the tilt angle  $\beta_{\text{tilt}}$  from the XRD rocking curve [16]. The twist angle  $\beta_{\text{twist}}$  was estimated according to the method outlined previously by Lee et al. [17].

$$\beta = \sqrt{(\beta_{\text{tilt}} \cos \chi)^2 + (\beta_{\text{twist}} \sin \chi)^2} \quad (2)$$

where the values of  $\beta$  were calculated for the FWHM values of the (102) reflection. The twist angle  $\beta_{\text{twist}}$  was calculated from XRD data according to Equation (2). The density of edge dislocations  $\rho_e$  was estimated using the following equation [16]:

$$\rho_e = \frac{\beta_{\text{twist}}^2}{4.35b_a^2} \quad (3)$$

where  $b_a$  is the Burgers vector of a-type TDs ( $b_a = 0.1503$  nm). Moreover, the Burgers vector of mixed dislocations (a + c)-types ( $b_m$ ) can be composed into pure screw and edge components:  $b_m = b_c + b_a$ . In this study, these dislocations are not considered separately [18]. Figure 7b shows the corresponding dislocation density determined from the DCXRD (002) and (102) reflections. At a growth time of 30 min, the AlGa<sub>N</sub> film on the NPSS exhibited a lower screw dislocation density of  $2 \times 10^9$  cm<sup>-2</sup> compared with that on the CSS ( $7 \times 10^9$  cm<sup>-2</sup>). Better crystallinity and lower TD might be attributed to the strain relaxation and dislocation reduction in the AlGa<sub>N</sub>/NPSS interface. To investigate the crystalline quality and local defect distribution of the AlGa<sub>N</sub> layer grown on the NPSS, TEM analysis was performed. Figure 7c presents a bright-field cross-sectional TEM image of the AlGa<sub>N</sub> layer grown on the NPSS under a two beam condition with  $g = 0002$ . The pure screw and mixed screw/edge defects are visible under the  $g = 0002$  two beam condition [19]. From the unpatterned substrate region,



a large number of typical extended TDs propagated throughout the AlGa<sub>x</sub>N film, originating at the interface between the AlGa<sub>x</sub>N and sapphire. These TDs were generated by the large lattice mismatch between the AlGa<sub>x</sub>N and sapphire. However, the voids and TDs bending observed within the NPSS indicate freestanding overgrowth in the lateral direction. Finally, TDs in the region above these voids were seldom observed. The results of TEM analysis indicate that the AlGa<sub>x</sub>N growth on the NPSS effectively reduced TDs in the epitaxial layer. This observation is similar to that reported in previous studies of PSS/ELOG [20].

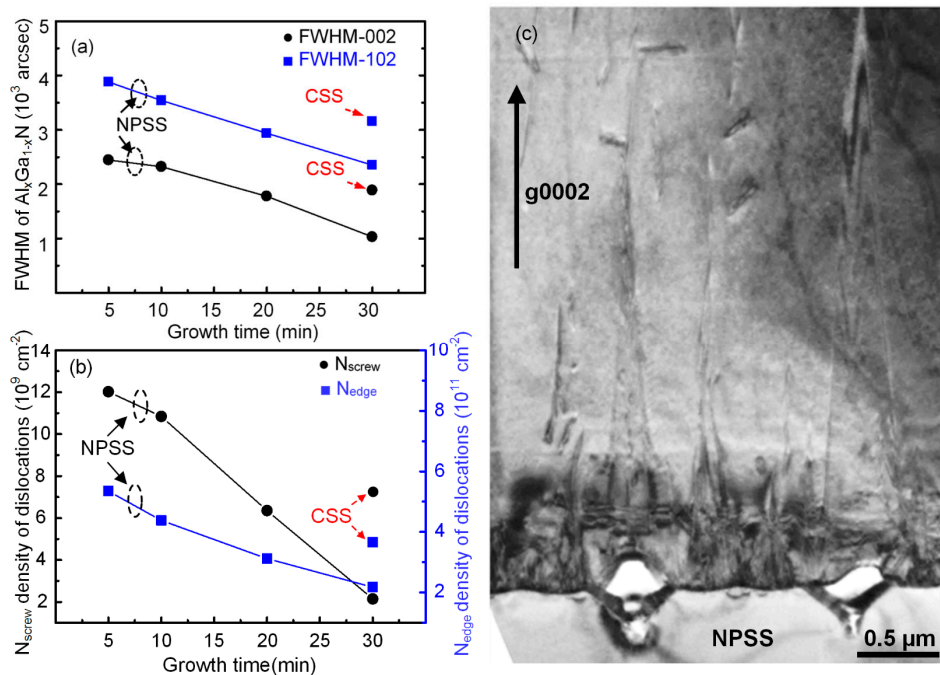


**Figure 7.** (a) Double-crystal x-ray diffraction (DCXRD) full-widths at half-maximum (FWHMs) of (0002)- and (10-12)-AlGa<sub>x</sub>N on NPSSs for various growth times (5, 10, 20, and 30 min); (b) Calculated screw and edge dislocation densities of AlGa<sub>x</sub>N samples on NPSSs for various growth times. The data for HVPE AlGa<sub>x</sub>N sample grown on a CSS for 30 min are also depicted for comparison; (c) Bright field TEM image of 3-μm-thick AlGa<sub>x</sub>N epilayer grown on an NPSS with  $g = 0002$ . The corresponding threading dislocation densities in various depths are also measured.

A prime concern about the AlGa<sub>x</sub>N heteroepilayers is their optical properties revealed by photoluminescence (PL) measurements. Figure 8a–d show the room-temperature PL emission spectra of AlGa<sub>x</sub>N films grown on NPSSs for various growth times (5–30 min). For comparison, the PL spectra of the 3-μm-thick GaN and AlGa<sub>x</sub>N samples on CSSs by HVPE are also presented in Figure 8e,f, respectively. The intense peak corresponding to near-band-edge emission at approximately 350 nm is related to the growth of AlGa<sub>x</sub>N-on-NPSS sample, whereas 360.8 nm is related to GaN-on-CSS and 353.5 nm is related to AlGa<sub>x</sub>N-on-CSS samples. As the growth time increased from 10 to 30 min, a redshift from 348 to 350 nm in the PL emission peak position was observed, corresponding to the grain-size confinement effect [21]. The redshift of the PL emission from 350 to 353.5 nm could be due to stress relaxation, where the AlGa<sub>x</sub>N-on-CSS sample with a higher TD density has been confirmed as compared with the AlGa<sub>x</sub>N-on-NPSS one (Figure 7b). Moreover, the PL peak intensity increased with increasing growth time. The increase in the PL peak intensity accompanied by the decrease in the number of defects indicates an improvement of the crystalline quality of the AlGa<sub>x</sub>N epilayer and a reduction of the defect density. The PL measurements indicate that the crystallinity and optical quality of the AlGa<sub>x</sub>N films grown on NPSSs improved with increasing growth time.

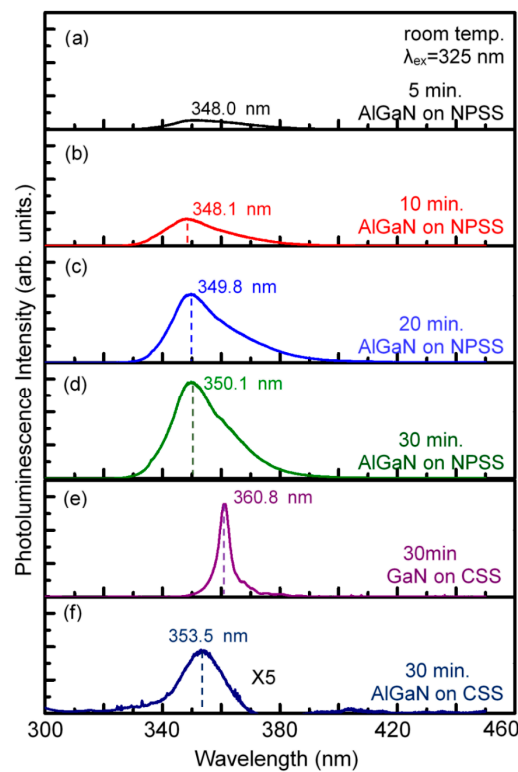


**Figure 8.** Room-temperature photoluminescence spectra of the HVPE AlGaN-on-NPSS epilayers as a function of growth time (a) 5; (b) 10; (c) 20 and (d) 30 min. The HVPE GaN and AlGaN samples on CSS for 30 min are also presented in (e,f) for comparison.

#### 4. Conclusions

In this study, the growth mechanism and crystal quality of AlGaN epilayers grown on NPSSs were investigated. SEM images revealed the dominant growth of (11–22) plane AlGaN from m-plane sidewalls of the NPSSs, and optical transmittance spectrum measurements showed that the AlGaN epilayer exhibited UV transparency for wavelengths above 360 nm. TEM analysis revealed that the annihilation of TDs was related to the formation of stacking faults resulting from the different strains present at the grain boundary between the AlGaN and NPSS. These results demonstrate the high potential of HVPE AlGaN/NPSS as the epitaxial template for fabricating high-performance AlGaN-based optoelectronics devices.

**Acknowledgments:** This work was supported by the Ministry of Science and Technology (Taiwan, R.O.C.) under Contract No. 104-2622-E-005-005-CC2 and 103-2622-E-005-009-CC2. The authors wish to express their sincere gratitude for the financial and technical support from the advanced Industry Technology Centre of National Chung Hsing University, Taiwan.

**Author Contributions:** D.S. and R.H. proposed the concept. C.T., T.Y. and R.H. conceived and designed the experiments. C.T., W.K. and S.Y. contributed the films measurement results. C.T., W.K. and D.S. wrote the manuscript. All authors read and approved the final version of the manuscript to be submitted.

**Conflicts of Interest:** The authors declare no conflict of interest.

#### References

1. Kneissl, M. *A Brief Review of III-Nitride UV Emitters in III-Nitride Ultraviolet Emitters: Technologies and Applications*; Kneissl, M., Rass, J., Eds.; Springer: Berlin, Germany, 2016; Chapter 1.
2. Shur, M.S.; Gaska, R. Deep-ultraviolet light-emitting diodes. *IEEE Trans. Electron Devices* **2010**, *57*, 12–25. [[CrossRef](#)]

3. Muramoto, Y.; Kimura, M.; Nouda, S. Development and future of ultraviolet light-emitting diodes: UV-LED will replace the UV lamp. *Semicond. Sci. Technol.* **2014**, *29*, 084004. [[CrossRef](#)]
4. Ban, K.; Yamamoto, J.I.; Takeda, K.; Ide, K.; Iwaya, M.; Takeuchi, T.; Kamiyama, S.; Akasaki, I.; Amano, H. Internal quantum efficiency of whole-composition-range AlGaN multi-quantum wells. *Appl. Phys. Express* **2011**, *4*, 052101. [[CrossRef](#)]
5. Imura, M.; Nakano, K.; Narita, G.; Fujimoto, N.; Okada, N.; Balakrishnan, K.; Iwaya, M.; Kamiyama, S.; Amano, H.; Akasaki, I.; et al. Epitaxial lateral overgrowth of AlN on trench-patterned AlN layer. *J. Cryst. Growth* **2007**, *298*, 257–260. [[CrossRef](#)]
6. Hennig, C.; Richter, E.; Weyers, M.; Tränkle, G. Self-separation of thick two inch GaN layers grown by HVPE on sapphire using epitaxial lateral overgrowth with masks containing tungsten. *Phys. Status Solidi C* **2007**, *4*, 2638–2641. [[CrossRef](#)]
7. Kumagai, Y.; Nagashima, T.; Murakami, H.; Takada, K.; Koukitu, A. Characterization of a freestanding AlN substrate prepared by hydride vapor phase epitaxy. *Phys. Status Solidi C* **2008**, *5*, 1512–1514. [[CrossRef](#)]
8. Koukitu, A.; Satoh, F.; Yamane, T.; Murakami, H.; Kumagai, Y. HVPE growth of Al<sub>x</sub>Ga<sub>1-x</sub>N ternary alloy using AlCl<sub>3</sub> and CaCl. *J. Cryst. Growth* **2007**, *305*, 335–339. [[CrossRef](#)]
9. Mogilatenko, A.; Hagedorn, S.; Richter, E.; Zeimer, U.; Goran, D.; Weyers, M.; Tränkle, G. Predominant growth of non-polar a-plane (Al,Ga)N on patterned c-plane sapphire by hydride vapor phase epitaxy. *J. Appl. Phys.* **2013**, *113*, 093505. [[CrossRef](#)]
10. Fleischmann, S.; Richter, E.; Mogilatenko, A.; Unger, R.S.; Prasai, D.; Weyers, M.; Tränkle, G. Triangular-shaped sapphire patterning for HVPE grown AlGaN layers. *Phys. Status Solidi A* **2016**. [[CrossRef](#)]
11. Hagedorn, S.; Richter, E.; Zeimer, U.; Weyers, M. HVPE of Al<sub>x</sub>Ga<sub>1-x</sub>N layers on planar and trench patterned sapphire. *J. Cryst. Growth* **2012**, *353*, 129–133. [[CrossRef](#)]
12. Hagedorn, S.; Richter, E.; Zeimer, U.; Weyers, M. HVPE growth of thick Al<sub>0.45</sub>Ga<sub>0.55</sub>N layers on trench patterned sapphire substrates. *Phys. Status Solidi C* **2013**, *10*, 355–358.
13. Kuwano, K.; Kugiyama, Y.; Nishikouri, Y.; Sato, T.; Usui, A. Electron microscopy analysis of dislocation behavior in HVPE-AlGaN layer grown on a stripe-patterned (0001) sapphire substrate. *J. Cryst. Growth* **2009**, *331*, 3085–3088. [[CrossRef](#)]
14. Richter, E.; Fleischmann, S.; Goran, D.; Hagedorn, S.; John, W.; Mogilatenko, A.; Prasai, D.; Zeimer, U.; Weyers, M.; Tränkle, G. Hydride vapor-phase epitaxy of c-plane AlGaN layers on patterned sapphire substrate. *J. Electr. Mater.* **2014**, *43*, 814–818. [[CrossRef](#)]
15. Allerman, A.A.; Crawford, M.H.; Lee, S.R.; Clark, B.G. Low dislocation density AlGaN epilayers by epitaxial overgrowth of patterned templates. *J. Cryst. Growth* **2014**, *388*, 76–82. [[CrossRef](#)]
16. Dunn, C.G.; Kogh, E. Comparison of dislocation densities of primary and secondary recrystallization grains of Si-Fe. *Acta Metal.* **1957**, *5*, 548–554. [[CrossRef](#)]
17. Lee, S.R.; West, A.M.; Allerman, A.A.; Waldrip, K.E.; Follstaedt, D.M.; Provencio, P.P.; Koleske, D.D. Effect of threading dislocations on the Bragg peak widths of GaN, AlGaN, and AlN heterolayers. *Appl. Phys. Lett.* **2005**, *86*, 241904. [[CrossRef](#)]
18. Barchuk, M.; Holy, V.; Miljevic, B.; Krause, B.; Baumbach, T.; Hertkorn, J.; Scholz, F. X-ray diffuse scattering from threading dislocations in epitaxial GaN layers. *J. Appl. Phys.* **2010**, *108*, 043521. [[CrossRef](#)]
19. Heying, B.; Wu, X.H.; Keller, S.; Li, Y.; Kapolnek, D.; Keller, B.P.; DenBaars, S.P.; Speck, J.S. Role of threading dislocation structure on the x-ray diffraction peak widths in epitaxial GaN films. *Appl. Phys. Lett.* **1996**, *68*, 643–645. [[CrossRef](#)]
20. Wu, D.S.; Wang, W.K.; Wen, K.S.; Huang, S.C.; Lin, S.H.; Huang, S.Y.; Lin, C.F.; Horng, R.H. Defect reduction and efficiency improvement of near-ultraviolet emitters via laterally overgrown GaN on a GaN/patterned sapphire template. *Appl. Phys. Lett.* **2006**, *89*, 161105. [[CrossRef](#)]
21. Wang, Y.D.; Zang, K.Y.; Chua, S.J.; Tripathy, S.; Chen, P.; Fonstad, C.G. Nanoair-bridged lateral overgrowth of GaN on ordered nanoporous GaN template. *Appl. Phys. Lett.* **2005**, *87*, 251915. [[CrossRef](#)]

